Chapter 1. Overview

Notes:

- *Most of the material presented in this chapter is taken from Stahler and Palla (2004), Chap. 1.*

1.1 Stellar Nurseries: Orion

Although Orion is one the best known constellations, we refer here to a specific region located within the constellation that is an active site of star formation. This region is arbitrarily separated into two parts: Orion A and Orion B (see Figure 1.1 and Figure 1.2). These regions consist in effect of huge concentrations of gas and dust and are thus called **molecular clouds**. Because of its size and mass the Orion star-forming region(s) is called a **Giant Molecular Cloud**.

1.1.1 Giant Molecular Clouds

Because of its closeness to the Sun and its location on the sky the Orion star-forming region is the most studied example of what is called a giant molecular cloud (GMC, sometimes also called a **cloud complex**). For example, the Orion Molecular Cloud (OMC) spans about 120 pc on the sky and weighs on the order of $10^5\ M_\odot$. There are thousands of giant molecular clouds in the Galaxy. They are called *molecular clouds* because they are mainly composed of molecular gas (as opposed to atomic gas, for example). Their main component is molecular hydrogen (H_2), although many other molecular species can also be detected.

The fact that hydrogen exists in its molecular phase instead of its atomic phase is due, in part, to the very low temperatures that are found in most regions of a giant molecular cloud (or any molecular cloud, giant or not); we are talking here of temperature on the order 10 K (and up to several times that much). Because of the low temperatures the gas inhabiting the clouds will not radiate at optical wavelengths and will not thus be easily detected; this will be verified with the image shown in Figure 1.3. The gas (and the dust) can only be detected at much longer wavelengths (in the radio regime, at millimeter and submillimetre wavelengths, and the infrared). It is therefore to be expected that images of a given region taken in the optical and, say, at submillimetre wavelengths will look the same. For example, the cold molecular gas will appear dark in the optical but will emit profusely at well-defined wavelengths in the millimeter, etc. These differences are further reinforced by the presence of interstellar dust grains also present within molecular clouds. This is because the dust grains (of approximately $0.1\mu\text{m}$ in size) are extremely efficient at absorbing radiation at optical wavelengths and, therefore, obscuring potentially large regions on astronomical images. These obscured regions are commonly called dark clouds. As we will see later, the radiation energy absorbed by the grains at optical wavelengths heats them up and is reradiated at longer wavelengths (i.e., in the infrared and submillimetre wavelengths) where it is directly detected. In fact, *dust radiation in the infrared is a signpost for the presence of newly formed, or nascent, stars*.

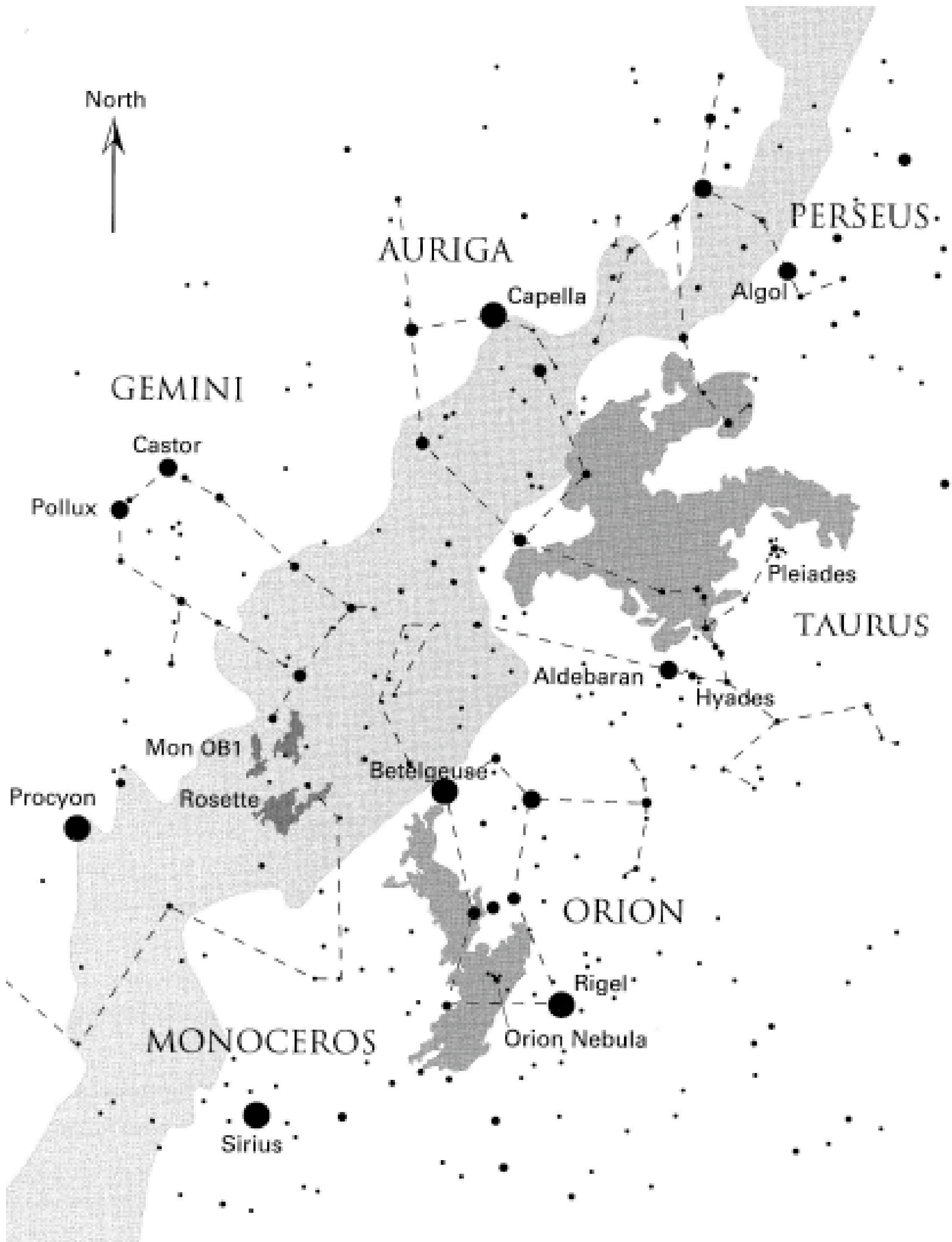

Figure 1.1 – A part of the Milky Way showing some well-known constellations and star formation regions.

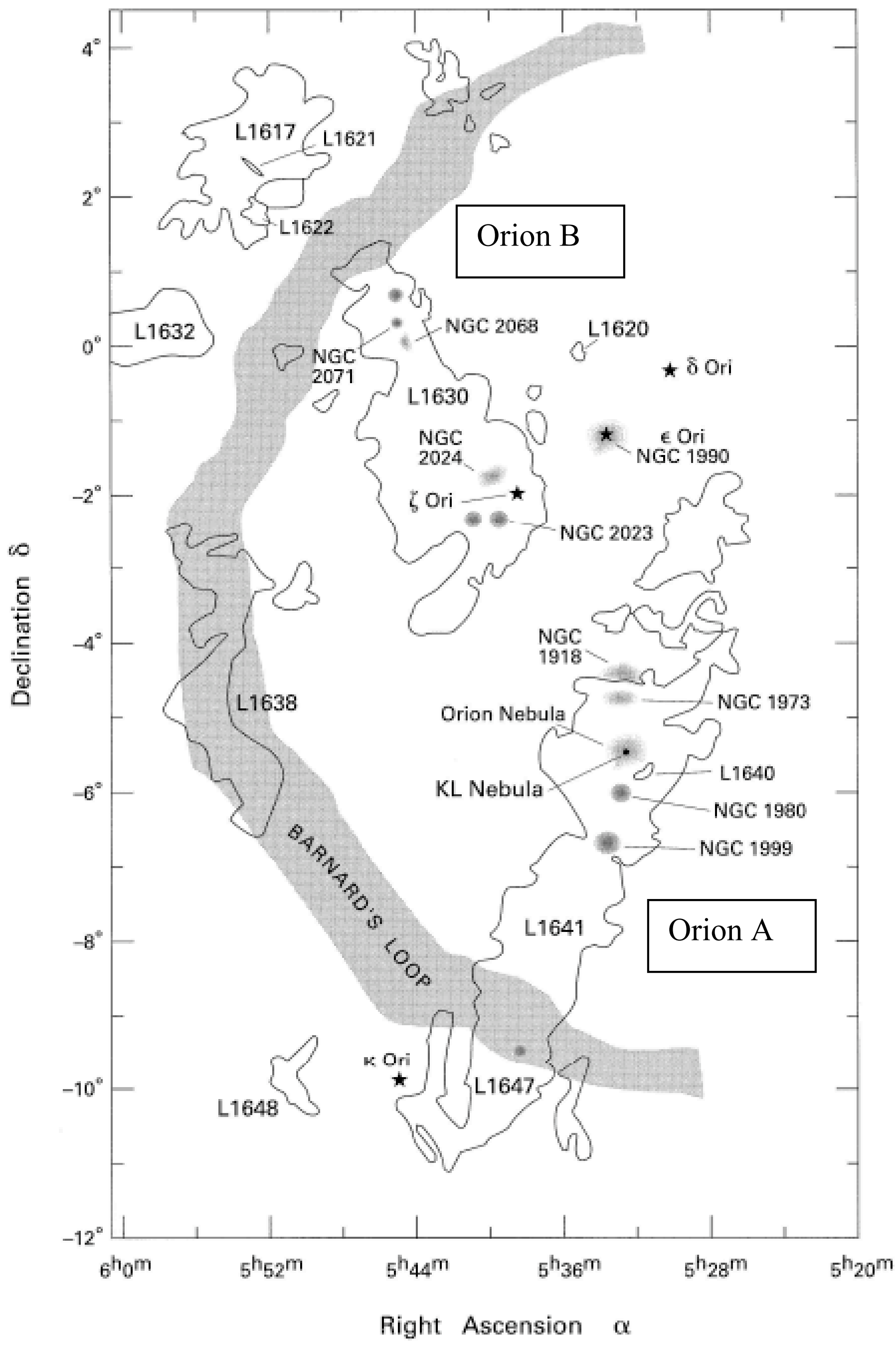

Figure 1.2 – A closer view of the Orion Molecular Cloud, the Orion A and B regions are identified. The dark patched are *reflection nebulae* (e.g., Orion Nebula and NGC 2071) and major molecular clouds (e.g., L1641) are labeled according to the *Lynds* catalog.

Figure 1.3 – An optical image of the Northern Sky from the Summit of Mauna Kea. Orion is seen rising on the right side of the picture (courtesy of Serge Brunier).

Figure 1.4 – Images of the Horsehead Nebula in Orion. The left image was obtained from carbon monoxide (i.e., CO) emission at approximately 345 GHz (or about $870\,\mu\mathrm{m}$). The other image is from the Hubble Space Telescope at optical wavelengths.

As can be guessed from Figure 1.4, molecular clouds are not smooth or homogeneous in structure or density, but rather clumpy. This is made evident when zooming in on the so-called Integral-shaped Filament of the Orion A cloud, as shown in Figure 1.5. The brightest region contained within the filament is the so-called Orion Nebula, which is shown in dust emission at $350\,\mu\text{m}$ and in the optical in Figure 1.6. As is often the case in parts of a GMC we find a cluster of massive and bright O and B stars (so-called OB associations) in the centre of the Orion Nebula. These stars are hot enough to radiate at ultraviolet wavelengths and ionized their surroundings, forming so-called HII regions. The name stem from the fact that the gas (or plasma) in HII regions is on the order of 10,000 K, which implies that not only molecules cannot form at these temperatures but that the atoms (mostly hydrogen) are ionized.

The Orion Nebula (also called M42, from the Messier Catalogue) is probably the most studied HII region. The group of OB stars that is responsible for the ionization is the Trapezium Cluster, which can be easily detected in the infrared (see Figure 1.7). As electrons recombine with protons within the plasma of the HII region they give rise to recombination lines. This allows us to measure the line-of-sight velocity of the plasma relative to the Sun (or to the observer). Along with similar measurements on molecular rotational lines emanating from the cloud we can reconstitute a model for this region. A simple representation is shown in Figure 1.8. More precisely, the OMC-1 region (for Orion Molecular Cloud-1) located behind the HII region of the Orion Nebula and the Trapezium are moving away from us at a velocity of 11 km/s along the line-of-sight, while the HII region is moving towards us at -3 km/s. Examples of molecular rotational lines detected in OMC-1 are shown in Figure 1.9; one notices that the line-of-sight velocity is approximately 11 km/s.

1.2 Stellar Nurseries: Taurus-Auriga

The Taurus-Auriga star-forming region is another example of molecular cloud. But it is different from that in Orion both because of its smaller size (30 pc at a distance of 140 pc versus 120 pc at a distance of 450 pc for OMC), and its smaller gaseous mass of $10^4\,M_\odot$. It is not a giant molecular cloud. Furthermore, the Taurus-Auriga cloud is known as a low-mass star-forming region. More precisely, it does not form or harbour any O and B types stars (i.e., there are no OB associations), and there are, therefore, no optical nebulae, which would result from the ionization of the gas and the ensuing formation of HII regions.

1.2.1 **Dark Clouds**

Because of the absence of reflection nebulae optical images of Taurus-Auriga will have totally different appearance than those of Orion. Such images distinguish themselves, however, by the presence of so-called dark clouds. These entities are dues to the obscuration of starlight form interstellar dust. Since the dust grains are coexistent with the gas with star-forming regions, it is expected that we should find a spatial coincidence between dark clouds and millimetre emission from molecules. This can be attested from Figure 1.10.

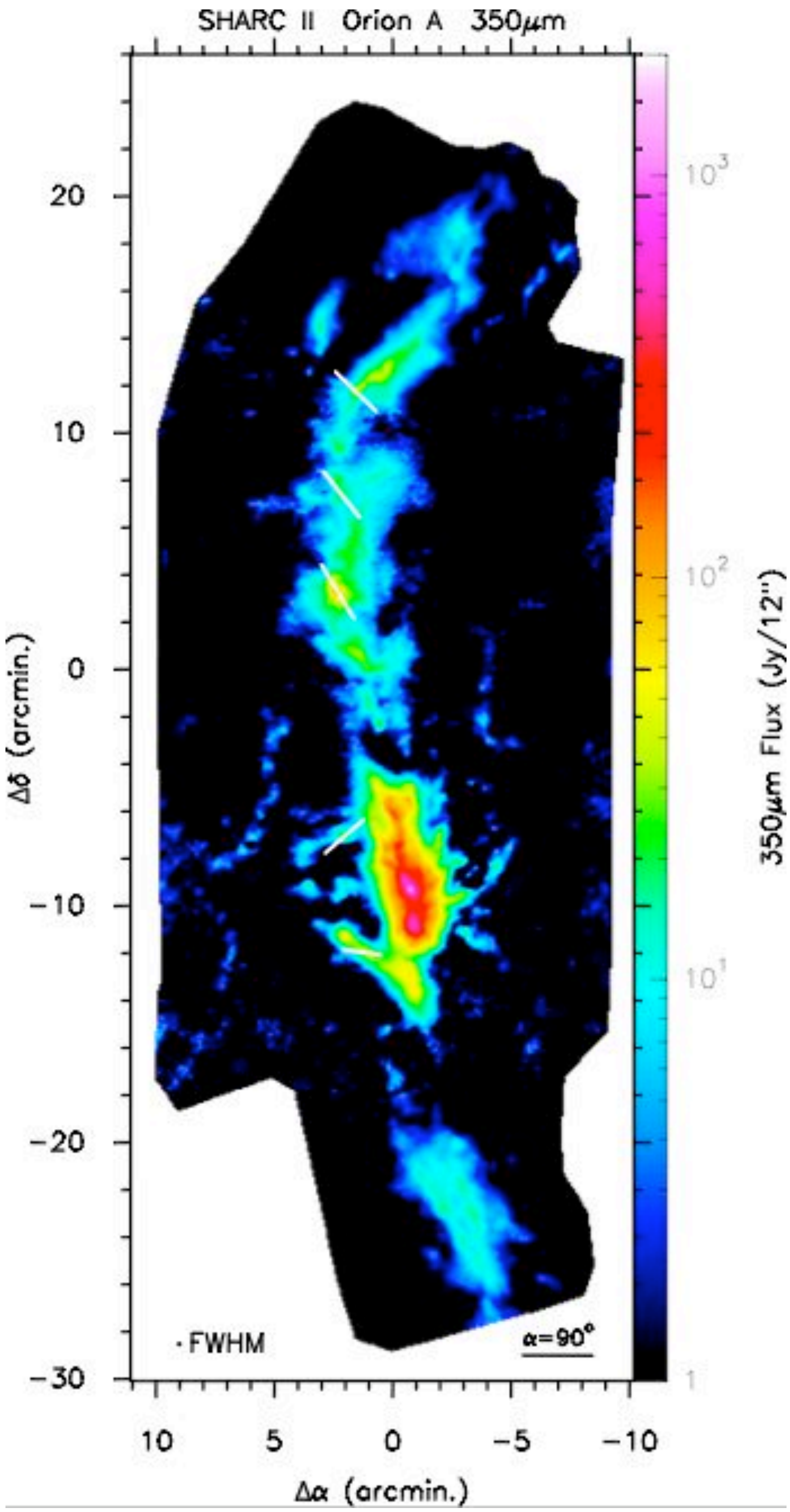

Figure 1.5 – The Orion Integral-shaped Filament as detected in dust continuum emission at $350\,\mu\text{m}$, at the Caltech Submillimeter Observatory (CSO). From Houde et al. 2004, ApJ, 604, 717.

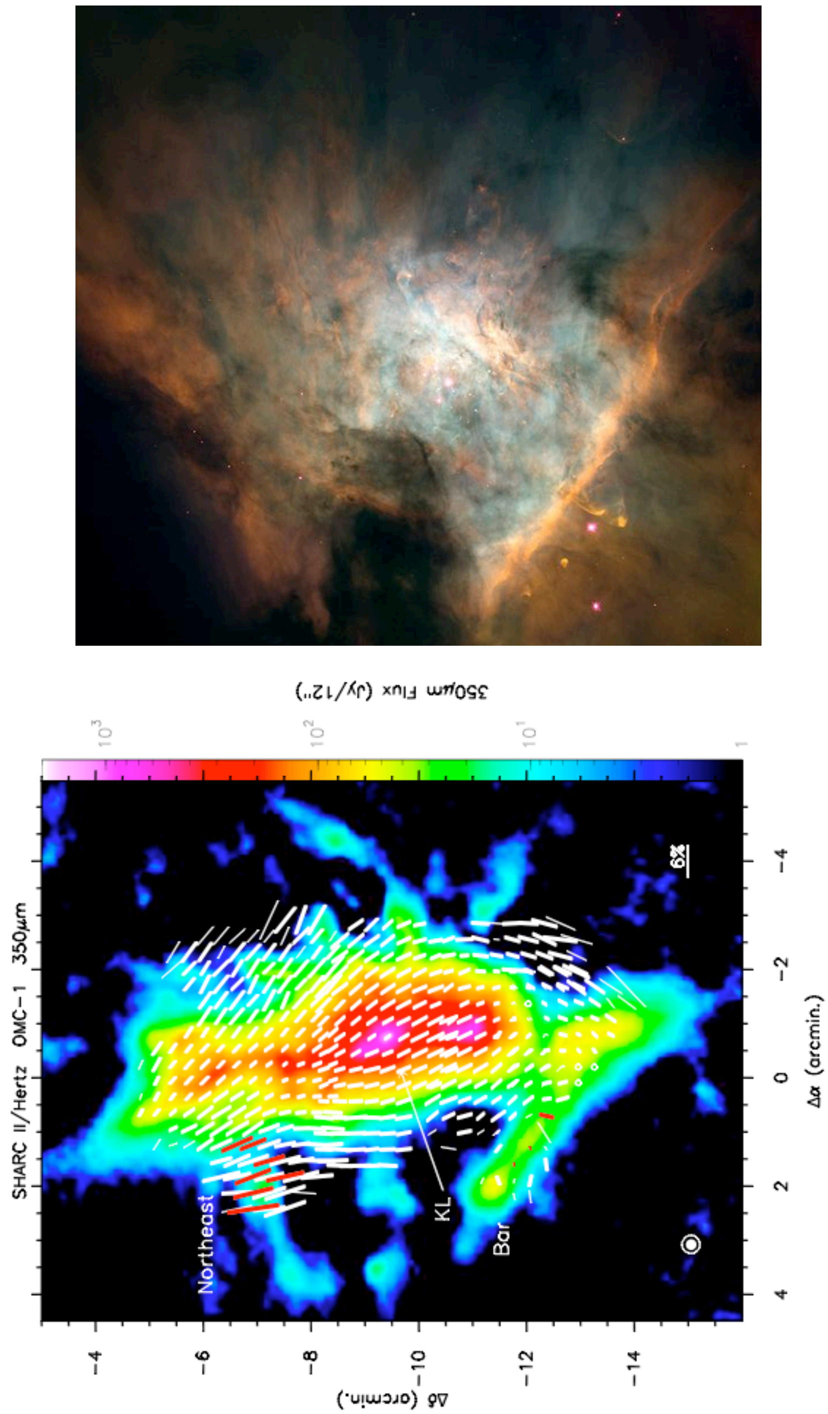

Figure 1.6 – The Orion Nebula as seen in dust emission at $350\,\mu$m (left) and in the optical (right). The bright stars visible at the centre are part of the Trapezium cluster.

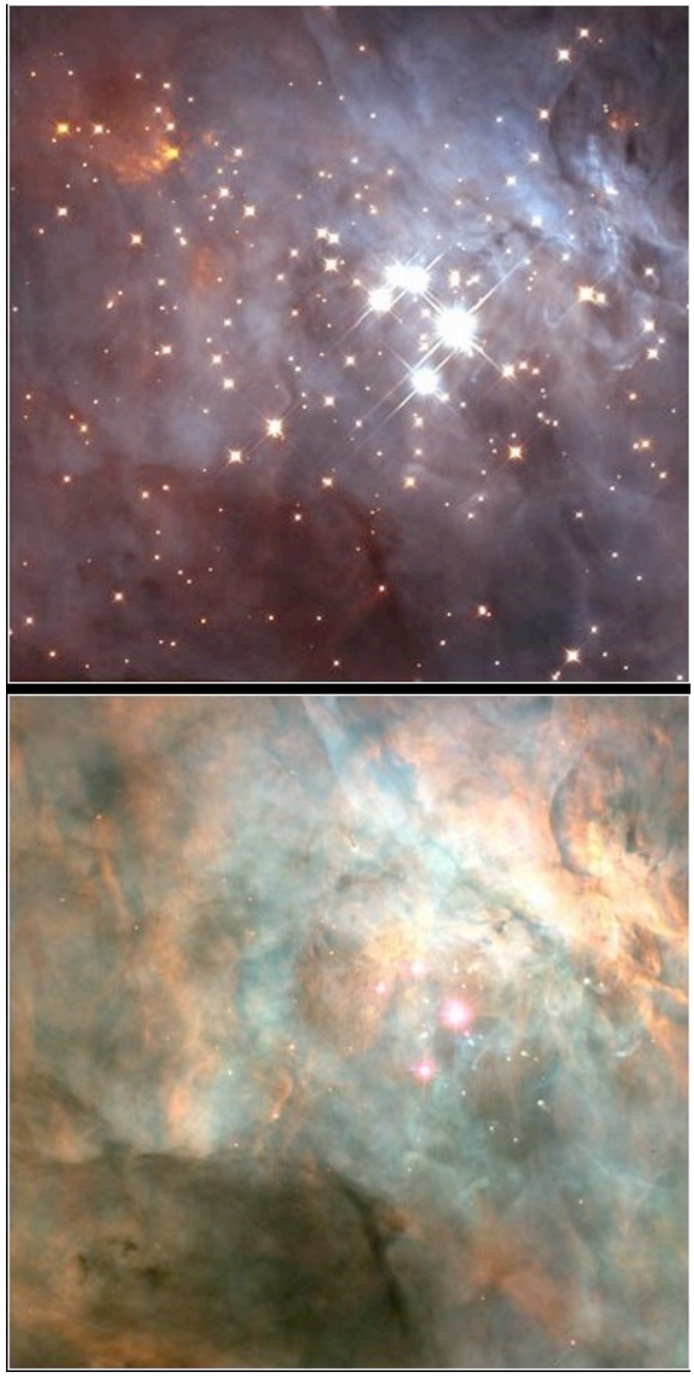

Figure 1.7 – The Trapezium cluster and newborn stars are easy to detect in the infrared (right) when we zoom into the centre of the Orion Nebula. The image on the left was taken at optical wavelengths.

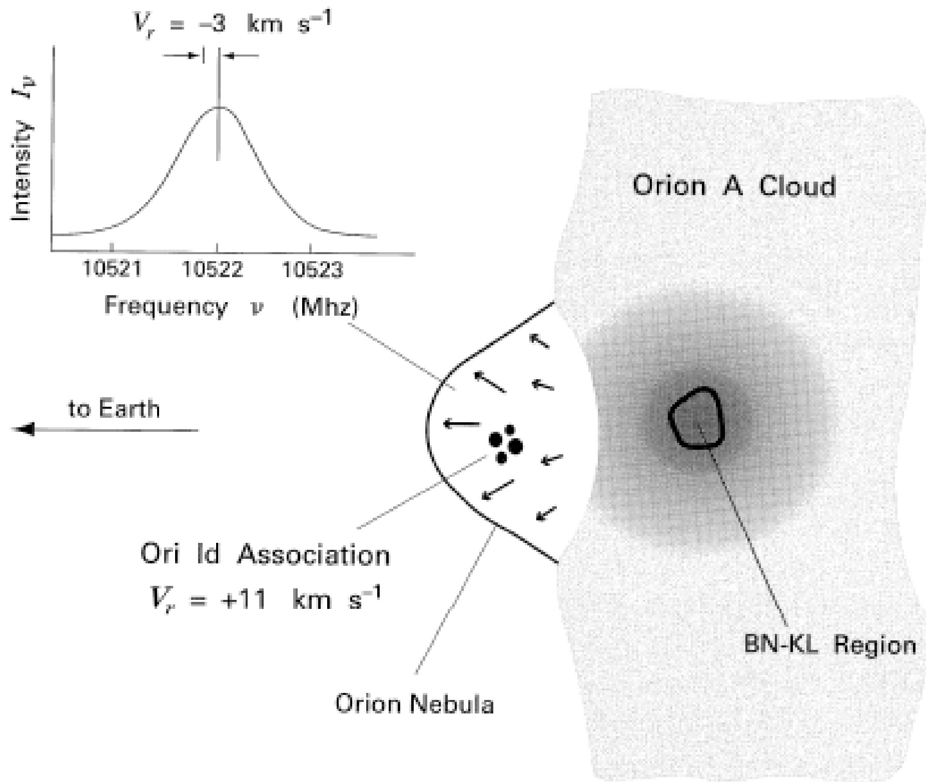

Figure 1.8 – A simplified model for the HII region of the Orion Nebula and the OMC-1 molecular cloud located behind it. OMC-1 and the Trapezium cluster are moving away from us at a velocity of 11 km/s along the line-of-sight, while the HII region is moving towards us at -3 km/s.

1.2.2 **T Associations**

Further inspection of the millimetre map of Figure 1.10 reveals the existence of an important number of so-called T Tauri stars, which are prototypical pre-main-sequence low-mass stars (observable in optical images), as well numerous infrared star (therefore enshrouded in dust, and young) and starless dense cores, which can only be observed at longer wavelengths (e.g., at millimetre and submillimetre wavelengths). The grouping of these different types stars within a region where dense molecular gas is also present, such as in the Taurus Molecular Cloud (TMC) is called a T association. In a way this is the low-mass counterpart to the OB associations observed in GMCs, such as in the OMC. Besides the absence of high-mass stars, another important aspect that differentiates T associations from OB associations is its more or less uniform spreading of the stars. For example, the stars in the Trapezium are extremely crowded (several hundred stars within a diameter of approximately 0.4 pc).

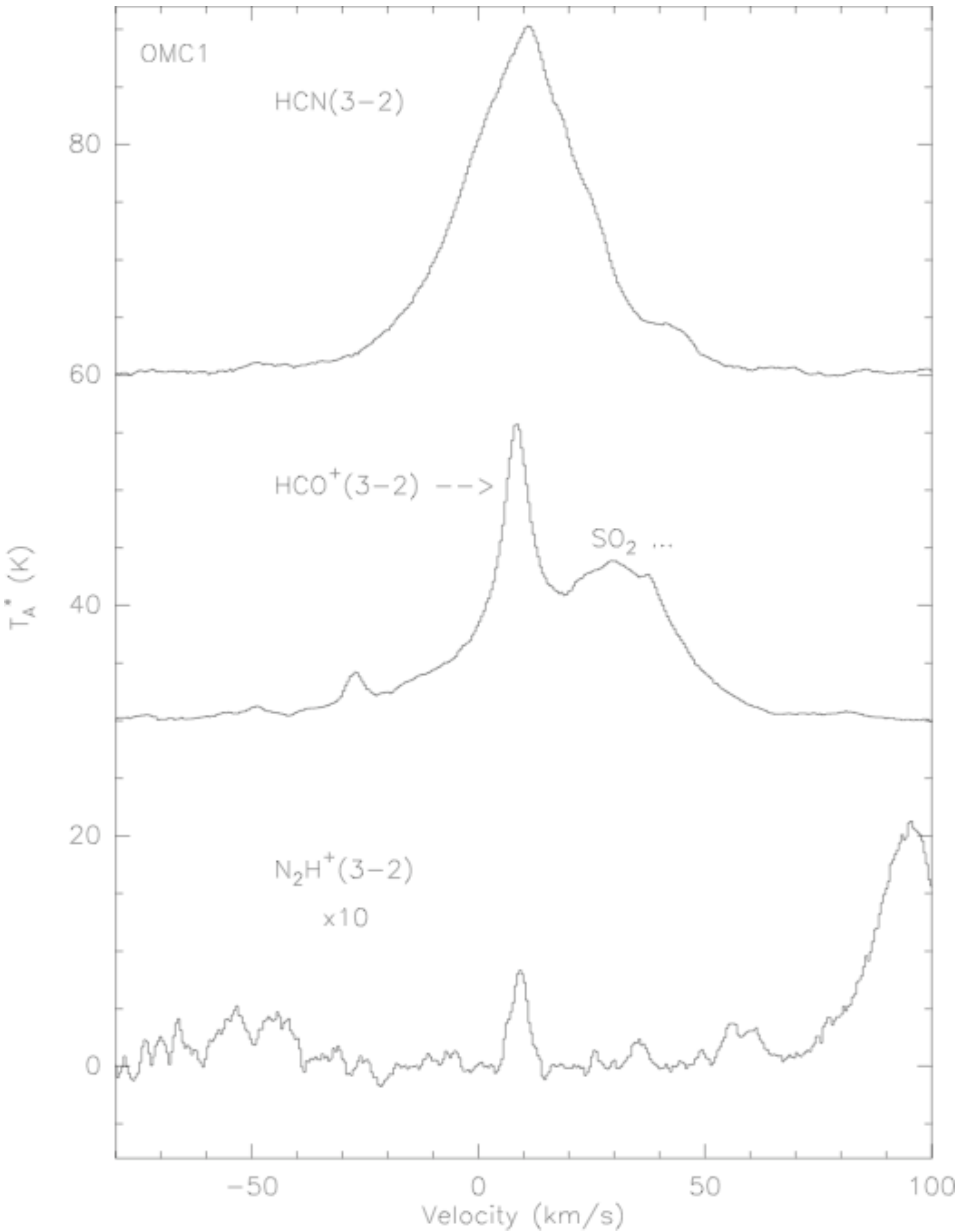

Figure 1.9 – Examples of molecular rotational lines detected in OMC-1. One notices that the line-of-sight velocity is approximately 11 km/s. From Houde et al. 2000, ApJ, 536, 857.

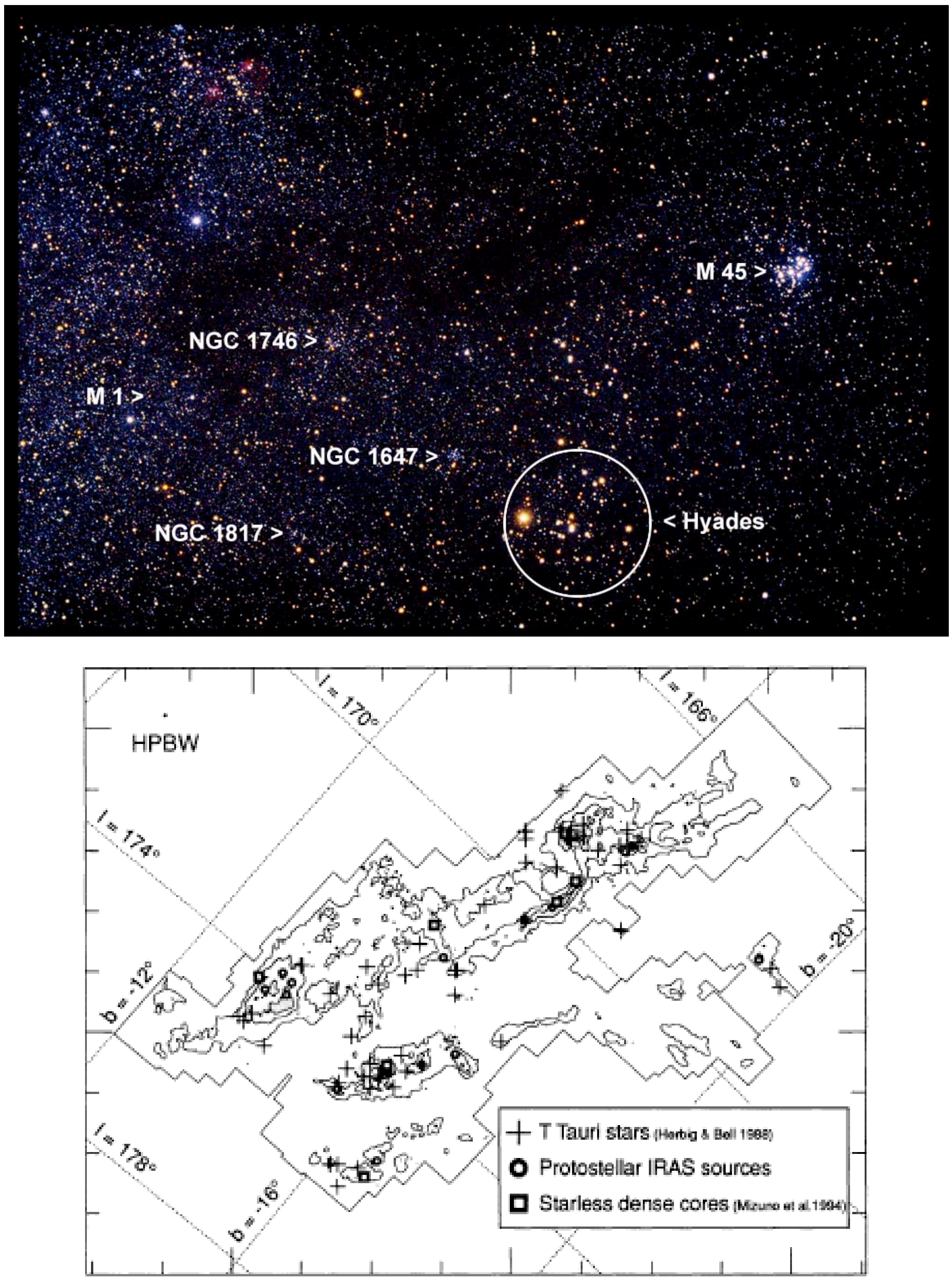

Figure 1.10 – Optical (top) and millimetre images (^{13}CO, bottom) of the Taurus-Auriga star-forming region. We see the spatial coincidence of darks clouds and submillimetre emission.

1.3 Stars and Their Evolution

As a protostar forms, the energy that is the source for its radiation is the gravitational energy that is released from its contraction. This contraction increases the density of the protostar with time, such that its **luminosity** L_* and its **effective temperature** T_{eff} continually change also (they increase as well). As it turns out, it is very difficult to gather direct observational evidence of gravitational contraction, but observations of mass ejections or outflows are ubiquitous. Because of this a protostar will eventually clear out the cocoon of dust and gas that surrounds it during its formation, and it becomes optically visible.

As the protostar emerges and becomes a pre-main-sequence star it becomes possible to measure its luminosity and determine its effective temperature. It is commonplace to construct graphs of luminosity versus effective temperature, both for pre-main-sequence and main sequence stars; this graph is the celebrated **Hertzsprung-Russel (HR) diagram**. In the case of pre-main-sequence stars, they appear on the HR diagram on the so-called **birthline**. The position of the star on the birthline curve is solely a function of its mass, as is shown in Figure 1.11. Accordingly, the gravitational contraction of the star will proceed at a rate that is also a function of its mass; the contraction and evolution as slow down as the mass is reduced.

A star possessing a mass superior to $0.08\,M_\odot$ will eventually reach a high enough centre temperature (approximately $10^7\,\mathrm{K}$) to allow the fusion of hydrogen nuclei into $^4\mathrm{He}$. At that point the star settles on the **Zero-Age Main Sequence (ZAMS)** at a position that is a function of its mass. The relationship between its luminosity and effective temperature is given by

$$L_* = 4\pi R_*^2 \sigma_{\mathrm{B}} T_{\mathrm{eff}}^4, \tag{1.1}$$

where R_* is the star's radius and σ_{B} the Stefan-Boltzmann constant. A measure of the time it takes a star to evolve from the birthline and the ZAMS is given by the so-called **Kelvin-Helmholtz time**

$$\begin{aligned} t_{\mathrm{KH}} &\equiv \frac{GM_*^2}{R_* L_*} \\ &= 3\times 10^7 \left(\frac{M_*}{M_\odot}\right)^2 \left(\frac{R_*}{R_\odot}\right)^{-1} \left(\frac{L_*}{L_\odot}\right)^{-1} \text{ yr}, \end{aligned} \tag{1.2}$$

where M_* is the star's mass. The evolution of a pre-main-sequence star from the birthline to the ZAMS as a function of mass and time is also shown in Figure 1.11.

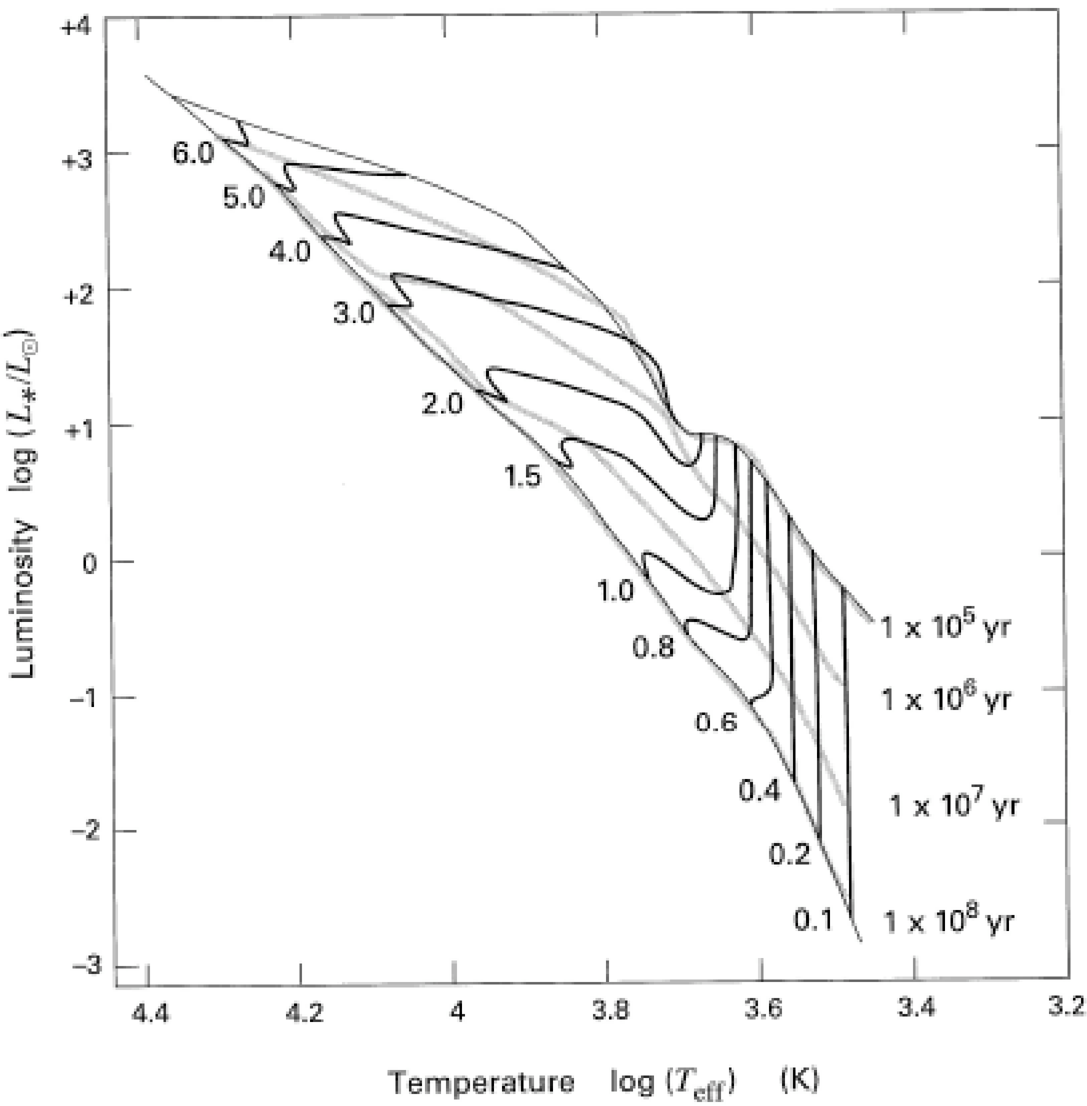

Figure 1.11 – Hertzsprung-Russel diagram showing the birthline of pre-main-sequence stars (upper solid line) and the Zero-Age Main Sequence (ZAMS) line (lower solid line), as well as the evolution between the two as a function of time and mass. Stars of higher masses emerge directly on the ZAMS. Please note that *the effective temperature increases leftward on the abscissa*.

A more complete view of the HR diagram is shown in Figure 1.12, along with the evolutionary track of a $1M_\odot$, from its appearance on the birthline to its transition on the ZAMS, and all the way to its demise as a white dwarf. If energy freed from gravitational contraction is the source for radiation for a protostar or a pre-main-sequence star, while a star reaches the main sequence it settles into "adulthood" in a state of hydrostatic equilibrium where internal pressure provides the needed support against gravity. Throughout the whole time it spends on the main sequence a star radiates at the constant rate L_*; it is also in thermal equilibrium. The energy lost to radiation is constantly replenished by the aforementioned fusion hydrogen nuclei into ^4He.

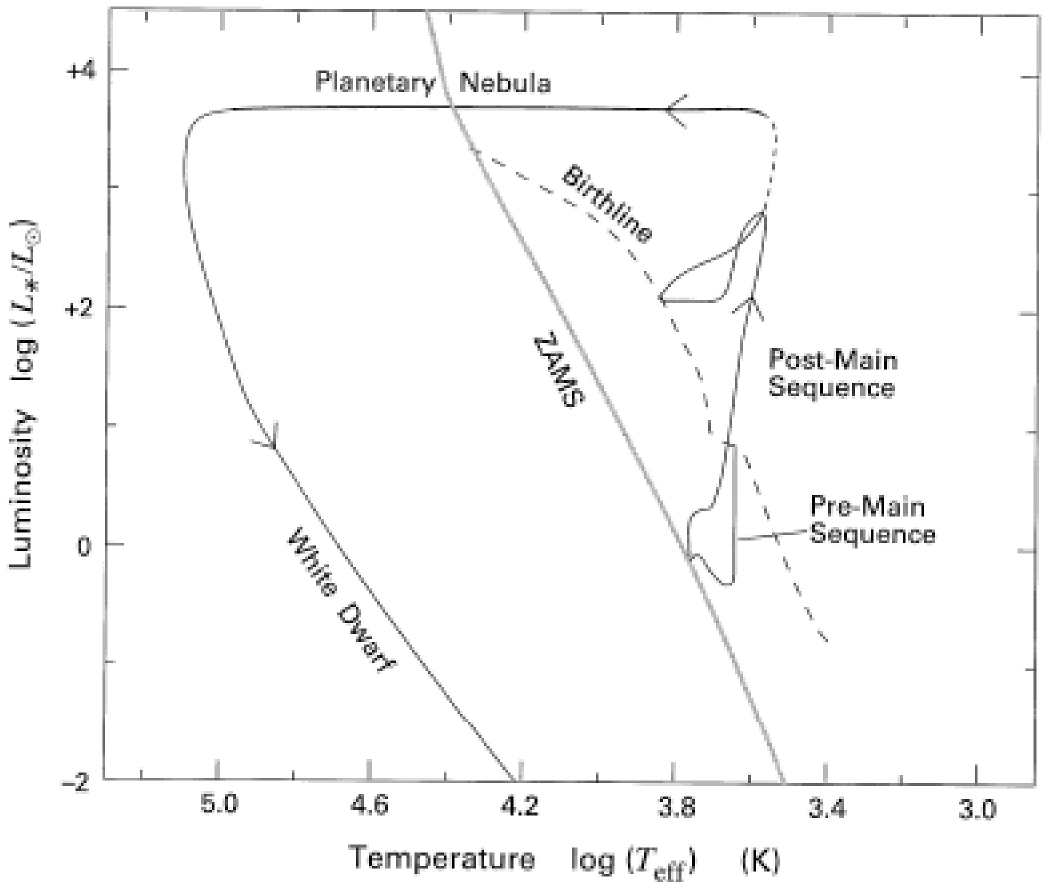

Figure 1.12 – A more complete look at the HR diagram, which clearly shows the birthline and the ZAMS. Also shown is the evolutionary track of a $1M_\odot$, from its appearance on the birthline to its transition on the ZAMS, and all the way to its demise as a white dwarf. Please note that *the effective temperature increases leftward on the abscissa*.

Because of the very large supply of hydrogen available in the interior of a star, a star will spend most of its life on the main sequence. It can be shown that its so-called **main sequence lifetime** $t_{\rm ms}$ is approximately given by

$$\begin{aligned} t_{\rm ms} &\approx 5\times 10^{-4}\,\frac{M_* c^2}{L_*} \\ &= 1\times 10^{10}\,\frac{\left(M_*/M_\odot\right)}{\left(L_*/L_\odot\right)}\ \text{yr.} \end{aligned} \tag{1.3}$$

It is easy to see from this relation that the Sun is expected to spend approximately 10 billion years on the main sequence; it is estimated to presently be 4.6 billions years old. In order to evaluate the main sequence lifetime for stars of different mass it is necessary to calculate the relationship between L_* and M_*.

Table 1.1 – Physical Properties of Main Sequence Stars.

Mass $(M_\odot)$	Spectral Type	M_V (mag)	$\log L_*$ $(L_\odot)$	$\log T_{\mathrm{eff}}$ (K)	t_{ms} (yr)
60	O5	-5.7	5.90	4.65	3.4×10^{6}
40	O6	-5.5	5.62	4.61	4.3×10^{6}
20	O9	-4.5	4.99	4.52	8.1×10^{6}
18	B0	-4.0	4.72	4.49	1.2×10^{7}
10	B2	-2.4	3.76	4.34	2.6×10^{7}
8	B3	-1.6	3.28	4.27	3.3×10^{7}
6	B5	-1.2	2.92	4.19	6.1×10^{7}
4	B8	-0.2	2.26	4.08	1.6×10^{8}
2	A5	1.9	1.15	3.91	1.1×10^{9}
1.5	F2	3.6	0.46	3.84	2.7×10^{9}
1	G2	4.7	0.04	3.77	1.0×10^{10}
0.8	K0	6.5	-0.55	3.66	2.5×10^{10}
0.6	K7	8.6	-1.10	3.59	
0.4	M2	10.5	-1.78	3.54	
0.2	M5	12.2	-2.05	3.52	
0.1	M7	14.6	-2.60	3.46	

The details of such calculations are beyond the scope of this course, but it can be shown (see Table 1.1) that the luminosity of a star increases much faster than its mass. This implies from equation (1.3) that more massive stars have a shorter lifetime. As can be seen from Table 1.1, a star of $60\,M_\odot$ (i.e., of spectral type O5) will only spend 3.4×10^{6} yr on the main sequence, while a $0.8\,M_\odot$ will last 2.5×10^{10} yr. In Table 1.1 the **absolute magnitude** M_V in the visual (V) band is defined as

$$M_V \equiv -2.5\log\left[F_V\left(10\text{ pc}\right)\right] + m_{V\circ}, \tag{1.4}$$

where $m_{V\circ}$ is a constant and $F_V\left(10\text{ pc}\right)$ is the radiation flux emanating and received from the star *if it were located at a distance of 10 pc*. It is important to note that brighter stars have a lower absolute magnitude. We also note in ending this section that it is common to substitute the **color-magnitude diagram** for the HR diagram. This consists of replacing the luminosity L_* by the absolute magnitude M_V, and the effective temperature T_{eff} by the **intrinsic color index**

$$\left(B-V\right)_\circ \equiv m_B - m_V, \tag{1.5}$$

where the magnitude m_B and m_V in the B and V bands, respectively, are assumed corrected for dust reddening. An example is shown in Figure 1.13.

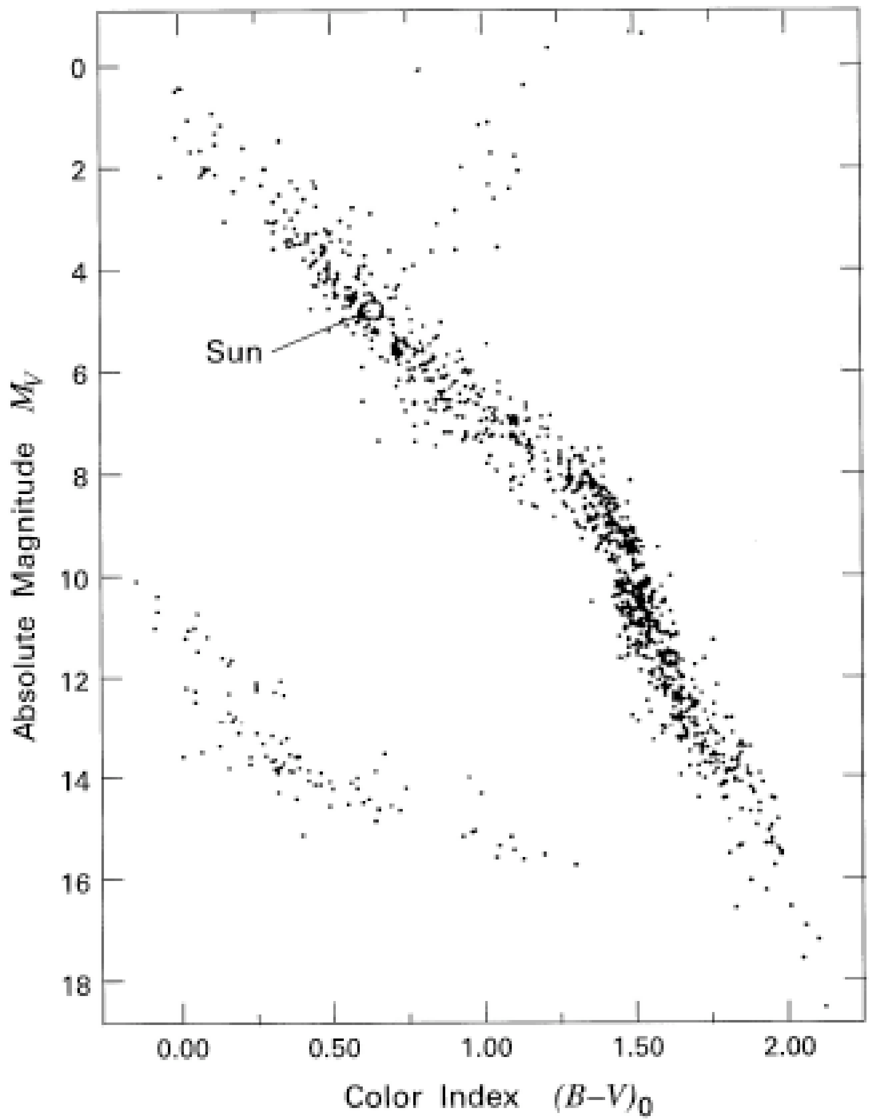

Figure 1.13 – Color-magnitude diagram for 1094 stars in the solar neighborhood. Please note that *the effective stellar temperature increases leftward on the abscissa*.

1.4 Recycling of Stars and Gas

As we have seen earlier, stars emanate from the gas that occupies the disk of our Galaxy. More precisely, gas is concentrated in entities we know as molecular clouds, which after localized contraction under its own self-gravity will eventually to the birth of stars. Although most of the gas in molecular clouds is composed of molecular hydrogen, there are also many other molecular species that can be detected (more than a hundred different species have been observed and identified so far, many others wait to be identified). Where do these molecules, which are often composed of heavier atoms, come from? Moreover, we also saw that dust grains coexist with the gas present in the clouds. Where does interstellar dust come form?

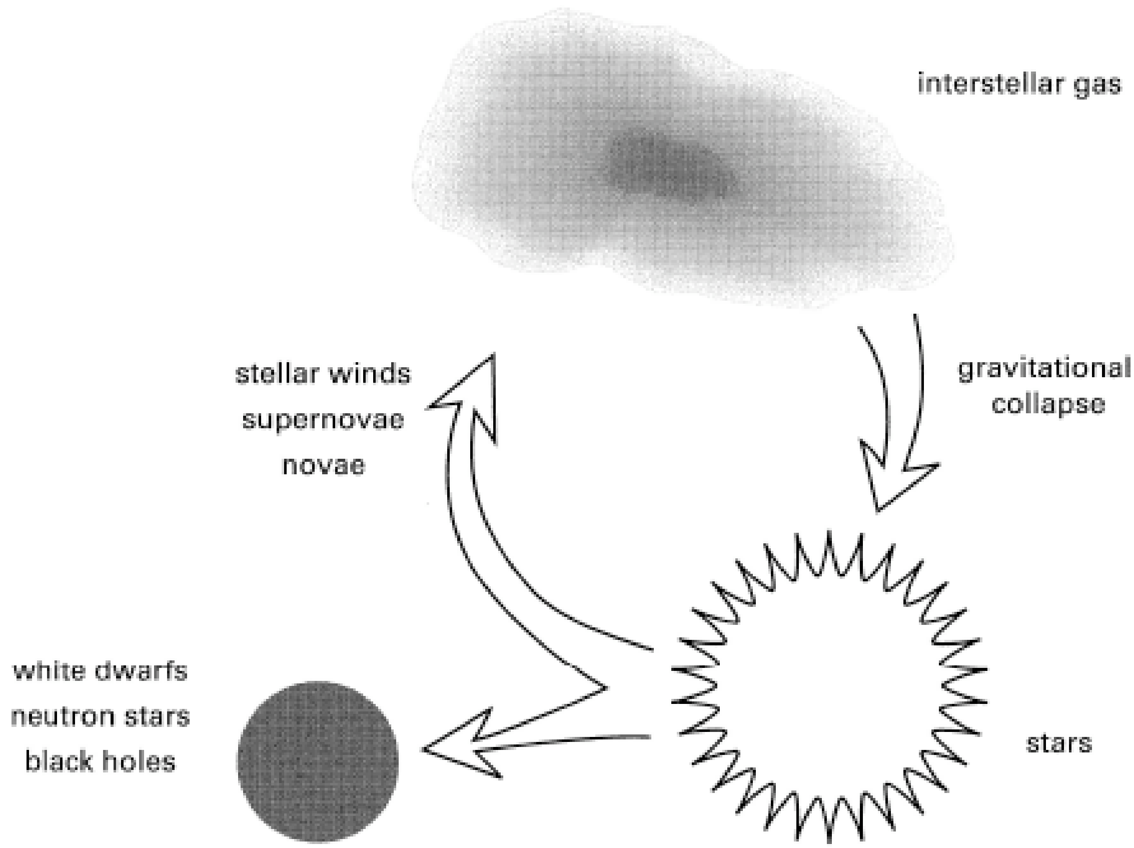

Figure 1.14 – Simplified representation of the recycling of stars and gas in the Galaxy.

As it turns out, stars re-inject a large part of the material used during their birth into the interstellar medium. Although all stars massive enough to undergo nuclear fusion in their centre will transform hydrogen nuclei into heavier nuclei, it is known that the most massive stars (of masses greater than approximately $8\,M_{\odot}$), which can become supernovae, are responsible for the production and the introduction of the heaviest nuclei in the interstellar medium. Obviously, this newly re-injected material will be used for the subsequent generation of stars to be formed in molecular clouds, and so on.

In the same manner, the interstellar dust grains originate in the circumstellar envelope of evolved star, which form after they have left the main sequence, to be thrown into the interstellar medium under the effect of stellar winds. These dusts grain then become an intrinsic part of the process of star formation.

It thus appears that the phenomenon of star formation is part of a huge recycling enterprise where interstellar material used in the formation of stars is transformed, processed, ejected, and reused for subsequent generations of stars. This is represented schematically in Figure 1.14.